Journal of Alloys and Compounds 506 (2010) 940–943

Contents lists available at ScienceDirect

Journal of Alloys and Compounds

journal homepage: www.elsevier.com/locate/jallcom

Raman study of 2H-$Mo_{1-x}W_xS_2$ layered mixed crystals

D.O. Dumcenco[a,1], K.Y. Chen[a], Y.P. Wang[a], Y.S. Huang[a,*], K.K. Tiong[b]

[a] Department of Electronic Engineering, National Taiwan University of Science and Technology, Taipei 106, Taiwan
[b] Department of Electrical Engineering, National Taiwan Ocean University, Keelung 202, Taiwan

ARTICLE INFO

Article history:
Received 18 January 2010
Received in revised form 14 July 2010
Accepted 16 July 2010
Available online 22 July 2010

PACS:
63.20.−e
63.22.−m
78.20.−e
78.30.−j

Keywords:
Semiconductors
Layered crystals
Raman scattering

ABSTRACT

A systematic study of a series of $Mo_{1-x}W_xS_2$ layered mixed crystals, with $0 \le x \le 1$, grown by the chemical-vapor transport method were carried out by using Raman scattering measurements. The peaks of the two dominant first-order Raman-active modes, A_{1g} and E^1_{2g}, and several second-order bands have been observed in the range of 200–1000 cm^{-1}. The peaks corresponding to A_{1g} mode show one-mode type behavior while the peaks of E^1_{2g} mode demonstrate two-mode type behavior for the entire series. The results can be explained on the basis of the atomic displacements for each mode. For A_{1g} mode only sulfur atoms vibrate and this give rise to a one-mode type behavior for the mixed crystals. For E^1_{2g} mode metal atoms also vibrate as well as sulfur atoms, the mass difference of the vibrating Mo and W cations causes the two-mode type behavior of E^1_{2g} mode. In addition, the observation of largest asymmetry and broadening of A_{1g} mode for $Mo_{0.5}W_{0.5}S_2$ has been attributed to random alloy scattering.

1. Introduction

Layered semiconductors TX_2 (T = Mo, W; X = S, Se, Te) are interesting due to their structural properties. In particular, the as crystallized two-dimensional layered-type structure can impart substantial anisotropy to most of their physical properties and have attracted investigators in an effort to acquire a better insight into the fundamental physics of these compounds [1–3]. The materials have also been extensively investigated because of the possible practical applications such as efficient electrodes in photoelectrochemical solar cells [4–6], catalysts in industrial applications and in secondary batteries [7–9], solid-state lubricants [10–12]. Over the last two decades, several papers concerning the preparation and characterization of $Mo_{1-x}W_xS_2$ compounds obtained by various methods have been published [13–17]. The X-ray studies confirmed that $Mo_{1-x}W_xS_2$ compounds synthesized directly from the constituent elements crystallized in a layered-type structure with hexagonal symmetry [13,14]. The thermal decomposition of thiometallate solid solutions $(NH_4)_2Mo_{1-x}W_xS_4$ in an inert or hydrogen atmosphere yields the formation of $Mo_{1-x}W_xS_2$ nanotubes and related structures [15–17]. Using piezoreflectance measurements in the vicinity of the direct band edge, it has been determined that the transition energies vary smoothly with the tungsten composition x, indicating that the natures of the direct band edges are similar for the $Mo_{1-x}W_xS_2$ compounds [14].

In this report, we present a systematic Raman scattering study of a series of $Mo_{1-x}W_xS_2$ layered mixed crystals grown by the chemical-vapor transport method. The peaks of the two dominant first-order Raman-active modes, A_{1g} and E^1_{2g}, and several second-order bands were observed. Polarization dependent measurements in the back-scattering configuration were performed to accurately determine the positions of A_{1g} and E^1_{2g} modes at different tungsten composition x. The peaks corresponding to A_{1g} mode show one-mode type behavior while the peaks of E^1_{2g} mode demonstrate two-mode type behavior for the entire series. The composition dependent behaviors of A_{1g} and E^1_{2g} modes are discussed.

2. Experimental

2.1. Single crystal growth

Single crystals of $Mo_{1-x}W_xS_2$ solid solutions were grown by the chemical-vapor transport method [14]. Prior to the crystal growth the powdered compounds of the series were prepared from the elements (Mo: 99.99%; W: 99.95% and S: 99.999%) by reaction at 1000 °C for 10 days in evacuated quartz ampoules. The W and Mo materials were added in such manner that the W composition x changing relatively to that of the molybdenum increases from 0 to 1 with a composition step size $\Delta x = 0.1$. The mixture was slowly heated to 1000 °C. This slow heating is necessary to avoid any explosions due to the strongly exothermic reaction between the elements. The

* Corresponding author at: Department of Electronic Engineering, National Taiwan University of Science and Technology, 43 Keelung Road, Section 4, Taipei 106, Taiwan. Tel.: +886 2 27376385; fax: +886 2 27376424.
E-mail address: ysh@mail.ntust.edu.tw (Y.S. Huang).
[1] Permanent address: Institute of Applied Physics, Academy of Science of Moldova, 5, Academiei str., MD-2028, Chisinau, Republic of Moldova.

0925-8388/$ – see front matter © 2010 Elsevier B.V. All rights reserved.
doi:10.1016/j.jallcom.2010.07.120

chemical transport was achieved with Br_2 as a transport agent in the amount of about 8 mg/cm^3. The growth temperature was set as 1030 → 980 °C with a temperature gradient of 3 °C/cm and a growth time of 20 days. The crystals had the shape of thin layer plates with thicknesses and surface areas ranging from 20 to 1000 μm and 20 to 100 mm^2, respectively. The weak interlayer van der Waals bonding means that they display good cleavage property parallel to the layers. X-ray analysis confirmed that the samples were single-phase materials of 2H-type structure over the entire range of the tungsten composition *x*. Electron probe microanalysis studies showed a chalcogen deficiency in the crystals and the existence of a small difference in composition between the crystals and the nominal starting compositions. For simplicity, the value of *x* henceforth is defined to be the nominal composition of the starting material.

2.2. Raman scattering

Raman measurements were achieved at room temperature utilizing the back-scattering configuration on a Renishaw inVia micro-Raman system with 1800 grooves/mm grating and an optical microscope with a 50× objective. A linearly polarized Ar^+ laser beam of the 514.5 nm excitation line with a power of ~1.5 mW was focused into a spot size ~5 μm in diameter. Prior to the measurement, the system was calibrated by means of the 520 cm^{-1} Raman peak of a polycrystalline Si.

3. Results and discussion

3.1. Background

Raman spectra of bulk 2H-TS_2 (T = Mo or W) have been studied extensively both experimentally and theoretically [18–21]. 2H-TS_2 belongs to the D^4_{6h} space group. It has 12 modes of lattice vibrations at the Γ point in the hexagonal Brillouin zone [18,20]. There are four first-order Raman-active modes in 2H-TS_2, corresponding to symmetries (the corresponding Raman shifts are in parentheses for MoS_2 and WS_2, respectively): E_{1g} (286 and 306 cm^{-1}), E^1_{2g} (383 and 356 cm^{-1}), A_{1g} (408 and 421 cm^{-1}) and E^2_{2g} (32 and 27 cm^{-1}) [19,21]. These modes have Raman polarization dependent tensors of the form [22]

$$\alpha(A_{1g}) = \begin{bmatrix} a & 0 & 0 \\ 0 & a & 0 \\ 0 & 0 & b \end{bmatrix};$$

$$\alpha(E_{1g}) = \begin{bmatrix} 0 & 0 & 0 \\ 0 & 0 & c \\ 0 & c & 0 \end{bmatrix}, \begin{bmatrix} 0 & 0 & -c \\ 0 & 0 & 0 \\ -c & 0 & 0 \end{bmatrix};$$

$$\alpha(E_{2g}) = \begin{bmatrix} 0 & d & 0 \\ d & 0 & 0 \\ 0 & 0 & 0 \end{bmatrix}, \begin{bmatrix} d & 0 & 0 \\ 0 & -d & 0 \\ 0 & 0 & 0 \end{bmatrix}. \quad (1)$$

In back-scattering experiments on a basal plane, i.e., on the surface perpendicular to the *c*-axis, the E_{1g} mode is forbidden whereas A_{1g} and E_{2g} ones are allowed [18,20]. Also, the E^2_{2g} mode, so-called the "rigid-layer" mode is expected in the region with very low-wavenumber value [20,23].

3.2. Raman spectra of 2H-MoS_2 and 2H-WS_2

Fig. 1 depicts the Raman spectra of 2H-MoS_2 and 2H-WS_2 samples in the range from 200 to 1000 cm^{-1} obtained with the incident laser light polarized perpendicular to the *c*-axis. The spectra reveal the first-order Raman signals as well as the second-order Raman (SOR) processes due to a coupling of phonons with non-zero momenta. Two prominent first-order Raman-active modes for 2H-TS_2 (T = Mo or W) single crystals designated as E^1_{2g} and A_{1g} are positioned in the range between 300 and 450 cm^{-1}. These modes are due to vibration of atoms within an S–T–S layer (see Fig. 2). For WS_2, we can observe a splitting of the Raman signal at around 355 cm^{-1} into two peaks at 352 and 356 cm^{-1}. Comparing the peak positions with the previous reports [19,21], the peak located at

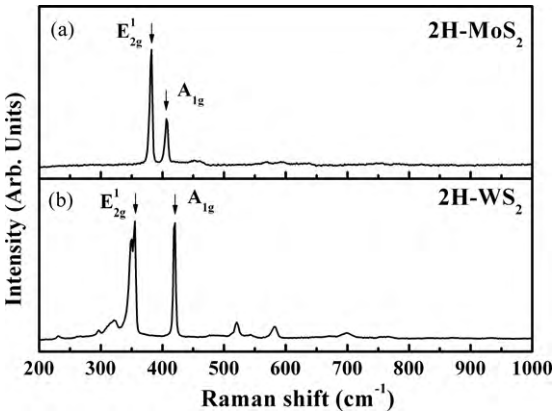

Fig. 1. Raman spectra of (a) 2H-MoS_2 and (b) 2H-WS_2 layered crystals in the range between 200 and 1000 cm^{-1}, showing the prominent E^1_{2g} and A_{1g} modes as well the second-order bands.

356 cm^{-1} is tentatively assigned as the first-order E^1_{2g} mode while the peak at 352 cm^{-1} is attributed to the SOR band due to the 2LA(K) overtone and will be discussed later. The other SOR bands can be assigned as combinations of sum or difference of bands involving phonons at the K point coupled to the LA(K) mode [24]. The energies and relative intensities of the observed peaks for both 2H-MoS_2 and 2H-WS_2 spectra corresponded well to the earlier reported well-known Raman modes [18–21].

3.3. Raman spectra of $Mo_{1-x}W_xS_2$ layered mixed crystals

To accurately determine the position of E^1_{2g} and A_{1g} modes as well as the SOR band located in the vicinity of E^1_{2g} of the tungsten containing samples, polarization dependent measurements in the back-scattering configuration had been carried out. The widely used Porto Notation method [25] for the designation of the crystal and polarization directions was utilized in this work. The [1 0 0], [0 1 0] and [0 0 1] crystallographic axes are being denoted by the letters *X*, *Y* and *Z*, respectively. The notation $Z(XX)\bar{Z}$ means the direction of incident radiation is along *Z*, the first and second terms in the bracket denotes the polarization of the incident and scattered light, respectively, and $\bar{Z}$ represents the direction of scattered light. For $Z(XX)\bar{Z}$ configuration, the analyzer placed just in front of the charge coupled device (CCD) camera was set to have polarization axis parallel to the polarization of the incident linearly polarized laser beam. A fine adjustment in the orientation of the [1 0 0] crystallographic axis of the sample to the **E** vector of the incident linearly polarized laser beam was made by the maximizing the intensity of the A_{1g} mode. The $Z(XY)\bar{Z}$ configuration was obtained simply by placing the half-wavelength plate directly between analyzer and CCD.

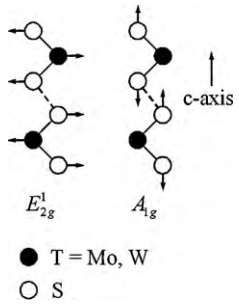

Fig. 2. Displacement of atoms for the Raman-active E^1_{2g} and A_{1g} modes in TS_2 (T = Mo or W) layered crystals of the 2H polytypes.

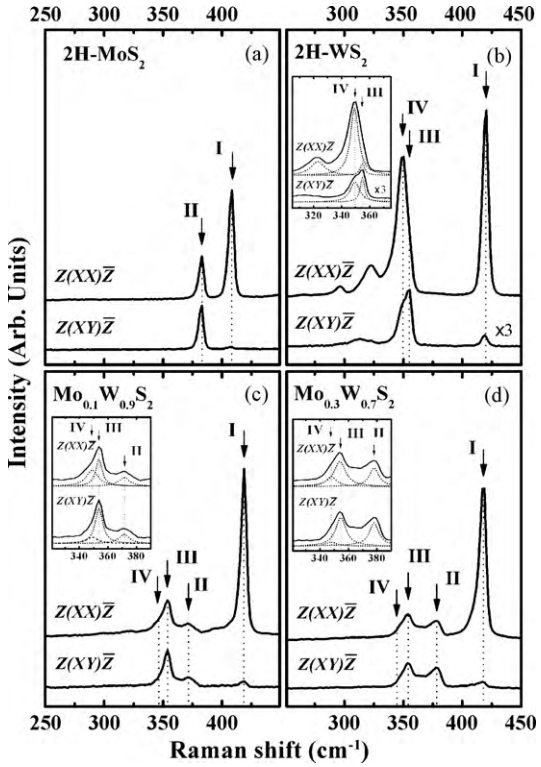

Fig. 3. Polarized Raman spectra of (a) MoS_2, (b) WS_2, (c) $Mo_{0.1}W_{0.9}S_2$ and (d) $Mo_{0.3}W_{0.7}S_2$ layered mixed crystals in the range from 250 to 450 cm^{-1} with $Z(XX)\bar{Z}$ and $Z(XY)\bar{Z}$ configurations. The dotted vertical lines show the position of the main peaks designating as I, II, III and IV. The insets in (b)–(d) show the lineshape fits in the vicinity of E^1_{2g} mode.

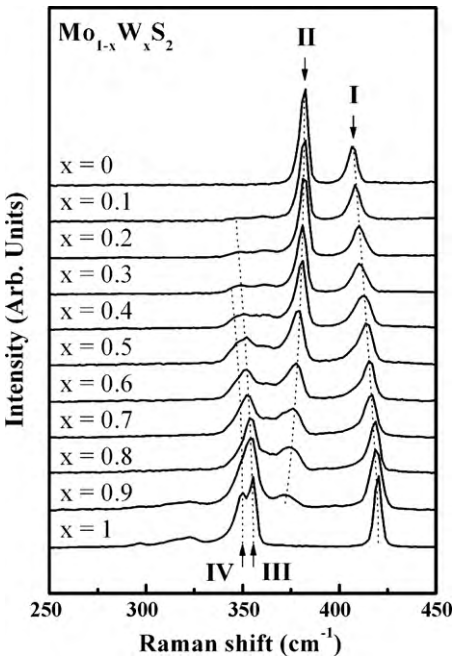

Fig. 4. Raman spectra of $Mo_{1-x}W_xS_2$ layered mixed crystals in the range between 250 and 450 cm^{-1}. The dotted lines guided by eyes show position dependence of the peaks with W compositions x.

The results of polarization dependent Raman spectra of several $Mo_{1-x}W_xS_2$ mixed crystals in the wavenumber range between 250 and 450 cm^{-1} are shown in Fig. 3. The intensity of Raman lines in $Z(XX)\bar{Z}$ and $Z(XY)\bar{Z}$ configurations differ appreciably showing the strong polarization dependence of the first-order Raman-active modes. In this wavenumber range, for 2H-MoS_2 single crystal (Fig. 3(a)), the peak denoted by I corresponds to A_{1g} mode is detected for $Z(XX)\bar{Z}$ configuration and quenched almost completely for that of $Z(XY)\bar{Z}$ configuration. The lower lying peak denoted by II is associated to E^1_{2g} mode and is observed both for $Z(XX)\bar{Z}$ and $Z(XY)\bar{Z}$ polarization configurations. Furthermore, the measured intensities of peak II for both $Z(XX)\bar{Z}$ and $Z(XY)\bar{Z}$ polarization revealed very similar value. The obtained results together with the strong polarization dependence agree well with the selection rules of E^1_{2g} and A_{1g} modes as given by the Raman scattering tensors α [22]. For the 2H-WS_2 sample (see Fig. 3(b)), a similar polarization behavior for higher wavenumber peak I is observed and assigned to be the A_{1g} mode. The lower lying structure is determined to be composed of two peaks positioning at 356 cm^{-1} (designated as III) and 352 cm^{-1} (designated as IV) in the $Z(XX)\bar{Z}$ configuration. A clear resolution of this structure can be seen in the unpolarized Raman spectrum of 2H-WS_2 as depicted in Fig. 1(b) and for the $Z(XY)\bar{Z}$ configuration in the polarized spectra (Fig. 3(b)). The relative intensities for peak III–IV in the $Z(XY)\bar{Z}$ configuration is larger than that of the $Z(XX)\bar{Z}$ configuration. This observation agrees with that reported by Sekine et al. [20]. Hence, the peak at 356 cm^{-1} is assigned to be the E^1_{2g} mode, while the peak at 352 cm^{-1} is attributed to be a second-order band. For the mixed $Mo_{1-x}W_xS_2$ samples, the assignment of peaks I and II can be facilitated by comparing their locations and polarization dependence with that of the binary end crystals while the relation of the relative intensities of peaks III and IV in the polarized Raman spectra has been utilized for the assignment (Fig. 3(c) and (d)).

Fig. 4 represents the Raman spectra of $Mo_{1-x}W_xS_2$ in the range from 250 to 450 cm^{-1}. As shown in Fig. 4, in the order from top to bottom, the value of the tungsten composition x increases from 0 to 1 with a composition step size $\Delta x = 0.1$ according to the stoichiometry of the constituent elements W and Mo. With W composition increasing, peak I moves to higher wavenumber. In contrast, as x value increases, peak II shifts to lower wavenumber with a reduction of peak intensity. Also with increasing of the tungsten composition, on the lower wavenumber side of Raman spectra of $Mo_{1-x}W_xS_2$, two additional peaks III and IV appear. Both of them demonstrate blue shift and become the dominant peaks at higher x values. It is noted that an alloy disorder-related peak [26] positioned in between peaks II and III is also observed for the mixed ternary $Mo_{1-x}W_xS_2$ samples.

The dependence of the wavenumbers of the Raman-active modes on the composition of $Mo_{1-x}W_xS_2$ layered mixed crystals are depicted in Fig. 5. For the A_{1g} mode, a one-mode behavior is the most typical, while for the E^1_{2g} mode, a two-mode behavior is observed. These experimental results can be explained satisfactorily on the basis of the atomic displacements for each mode; for A_{1g} mode only sulfur atoms vibrate and this give rise to a one-mode type behavior for the mixed crystals. For E^1_{2g} mode metal atoms also vibrate as well as sulfur atoms (see Fig. 2). The atomic weight of tungsten atom is 1.92 times larger than that of molybdenum one, and this mass difference most probably causes the two-mode type behavior of E^1_{2g} mode. These behaviors of the composition dependences are often seen in the Raman spectra of the solid solutions in which no ordered distribution of the constituent atoms exist [27,28].

The mixed crystals cannot have an ideal periodic lattice. As the composition of W increases, the disorder effect increases in the layered mixed crystals $Mo_{1-x}W_xS_2$, and the intensities of the modes related to 2H-MoS_2 decreases, while 2H-WS_2 associated modes increases. This finite periodicity in the mixed crystals relaxes the $q = 0$ Raman selection rule, thus leading to the broadening and

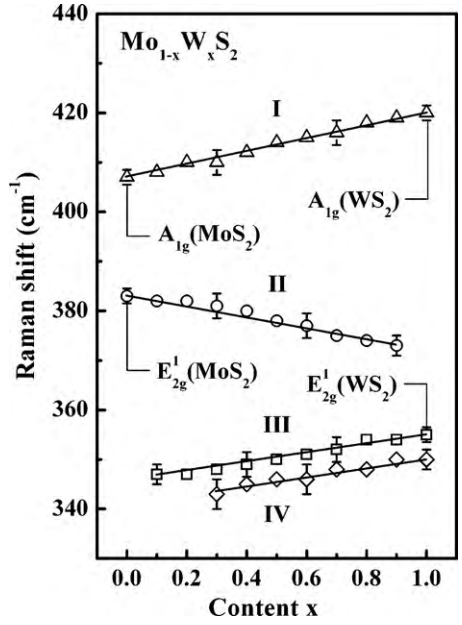

Fig. 5. The variation of peaks I, II, III and IV as a function of W composition x of $Mo_{1-x}W_xS_2$ layered mixed crystals.

asymmetry of the Raman lineshape. Symmetric phonon line of the A_{1g} mode for pure 2H-MoS_2 (Fig. 6(a)) and 2H-WS_2 (Fig. 6(c)) become asymmetric for $Mo_{1-x}W_xS_2$ mixed crystals (Fig. 6(b)). The low-wavenumber side half-width (Γ_{low}) is larger than the high-wavenumber side half-width (Γ_{high}). The ratio $\Gamma_{low}/\Gamma_{high}$ shows maximum at $x = 0.5$. This indicates that the mixed crystal disorder effect is the main source for the Raman lineshape change as a function of composition. At this point, it is worth noting that

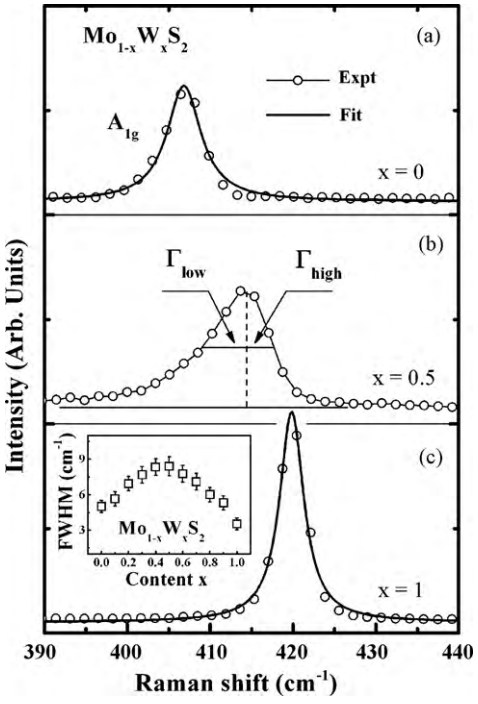

Fig. 6. Lineshape analysis of Raman spectra of A_{1g} mode for (a) MoS_2, (b) $Mo_{0.5}W_{0.5}S_2$ and (c) WS_2 layered crystals. The inset in (c) represents the W composition dependence of linewidth broadening of A_{1g} mode for the $Mo_{1-x}W_xS_2$ layered mixed crystals.

similar broadening and asymmetry of the phonon lines have been previously observed in $TlGa_xIn_{1-x}S_2$ layered mixed crystals [29]. The inset of Fig. 6(c) shows the composional dependence of the full width at half maximum (FWHM) for A_{1g} mode. It is noticed that FWHM values of the corresponding modes for MoS_2 layered crystals were found to be higher than those for WS_2 crystals. In addition, as expected, the FWHM dependence has maximum at $x = 0.5$, which corresponds maximum substitutional disorder in the mixed crystals.

4. Summary

The Raman spectra for $Mo_{1-x}W_xS_2$ layered mixed crystals were investigated for a wide range of the composition with $0 \le x \le 1$. The peaks of the two dominant first-order Raman-active modes, A_{1g} and E^1_{2g}, and several second-order bands have been observed in the range of 200–1000 cm^{-1}. The peaks corresponding to A_{1g} mode show one-mode type behavior while the peaks of E^1_{2g} mode demonstrate two-mode type behavior for the entire series. These results are explained on the basis of the atomic displacements for each mode. For A_{1g} mode only sulfur atoms vibrate and this give rise to a one-mode type behavior for the mixed crystals. While for E^1_{2g} mode, metal atoms also vibrate as well as sulfur atoms. The mass difference of the vibrating Mo and W cations causes the two-mode type behavior of E^1_{2g} mode. The largest FWHM value and asymmetry of A_{1g} mode at $x = 0.5$ are due to crystal disorder.

Acknowledgements

The authors would like to acknowledge the financial supports by the National Science Council of Taiwan under Grant Nos. NSC 97-2112-M-011-001-MY3 and 98-2811-M-011-003.

References

[1] J.A. Wilson, A.D. Yoffe, Adv. Phys. 18 (1969) 193–335.
[2] L.F. Mattheiss, Phys. Rev. B 8 (1973) 3719–3740.
[3] E. Fortin, F. Raga, Phys. Rev. B 11 (1975) 905–912.
[4] W. Kautek, H. Gerisch, H. Tributsch, J. Electrochem. Soc. 127 (1980) 2471–2478.
[5] K.K. Kam, B.A. Parkinson, J. Phys. Chem. 86 (1982) 463–467.
[6] S.J. Li, J.C. Bernède, J. Pouzet, M. Jamali, J. Phys.: Condens. Matter 8 (1996) 2291–2304.
[7] P. Grange, B. Delmon, J. Less-Common Met. 36 (1974) 353–360.
[8] P.G. Moses, B. Hinnemann, H. Topsøe, J.K. Nørskov, J. Catal. 248 (2007) 188–203.
[9] C.T. Tye, K.J. Smith, Catal. Today 116 (2006) 461–468.
[10] J.M. Martin, C. Donnet, J. Le Mogne, T. Epicier, Phys. Rev. B 48 (1993) 10583–10586.
[11] S.D. Walck, J.S. Zabinski, N.T. McDevitt, J.E. Bultman, Thin Solid Films 305 (1997) 130–143.
[12] L. Rapoport, V. Leshchinsky, I. Lapsker, Yu. Volovik, O. Nepomnyashchy, M. Lvovsky, R. Popovitz-Biro, Y. Feldman, R. Tenne, Wear 255 (2003) 785–793.
[13] S.K. Srivastava, T.K. Mandal, B.K. Samantaray, Synth. Met. 90 (1997) 135–142.
[14] C.H. Ho, C.S. Wu, Y.S. Huang, P.C. Liao, K.K. Tiong, J. Phys.: Condens. Matter 10 (1998) 9317–9328.
[15] C. Thomazeau, C. Geantet, M. Lacroix, V. Harlé, S. Benazeth, C. Marhic, M. Danot, J. Solid State Chem. 160 (2001) 147–155.
[16] C. Thomazeau, C. Geantet, M. Lacroix, M. Danot, V. Harlé, P. Raybaud, Appl. Catal. A: Gen. 322 (2007) 92–97.
[17] M. Nath, K. Mukhopadhyay, C.N.R. Rao, Chem. Phys. Lett. 352 (2002) 163–168.
[18] T.J. Wieting, J.L. Verble, Phys. Rev. B 3 (1971) 4286–4292.
[19] J.M. Chen, C.S. Wang, Solid State Commun. 14 (1974) 857–860.
[20] T. Sekine, T. Nakashizu, K. Toyoda, K. Uchinokura, E. Matsuura, Solid State Commun. 35 (1980) 371–373.
[21] C. Sourisseau, M. Fouassier, Mater. Sci. Eng. B 3 (1989) 119–123.
[22] R. Loudon, Adv. Phys. 13 (1964) 423–482.
[23] J.L. Verble, T.J. Wieting, P.R. Reed, Solid State Commun. 11 (1972) 941–944.
[24] C. Sourisseau, F. Cruege, M. Fouassier, M. Alba, Chem. Phys. 150 (1991) 281–293.
[25] T.C. Damen, S.P.S. Porto, B. Tell, Phys. Rev. 142 (1966) 570–574.
[26] S. Ould Saad Hamady, N. Dupuis, J. Décobert, A. Ougazzaden, J. Cryst. Growth 310 (2008) 4741–4746.
[27] M. Ishii, M. Saeki, Solid State Commun. 67 (1988) 895–898.
[28] I.F. Chang, S.S. Mitra, Adv. Phys. 20 (1971) 359–404.
[29] N.M. Gasanly, N.S. Yuksek, Acta Phys. Pol. A 108 (2005) 997–1003.